Mine Water and the Environment (2019) 38:767–779
https://doi.org/10.1007/s10230-019-00638-w

TECHNICAL ARTICLE

Method to Predict the Height of the Water Conducting Fractured Zone Based on Bearing Structures in the Overlying Strata

Feng Wang[1,2] · Jialin Xu[3,4] · Shaojie Chen[1,2] · Mengzi Ren[2]

Received: 27 April 2018 / Accepted: 30 September 2019 / Published online: 11 October 2019

Abstract

Numerous mining-induced water inrush hazards have been recorded in northern and eastern China, wherein landforms comprise thick unconsolidated layers. To prevent such hazards, the height of the water conducting fractured zone (WCFZ) must be determined in advance. This study presents a method to predict the height of this zone by determining the location of the key strata (KS) and considering the overburden load transfer under an arch structure in the unconsolidated layers. When the distance between the primary key stratum (PKS) and coal seam is more than 7–10 × M, where M refers to the mining height, the WCFZ tends to extend up to the floor level of the first KS, approximately the same distance (7–10 × M) above the mining seam, thereby making the height of this zone equal to the distance between the KS and coal seam. When the vertical distance between the PKS and coal seam is less than 7–10 × M, the height of this zone tends to be equal to or greater than the thickness of the bedrock strata. The theoretical results were verified by field observations.

Keywords Water inrush · Key strata · Arch structure in unconsolidated layers · Load reduction factor

Introduction

Underground Longwall (LW) coal mining operations are associated with numerous hazards, such as land subsidence (Xuan and Xu 2014), roof collapse (Xu 2016), coal and rock bursts (Cai et al. 2015), gas outbursts (Fisne and Esen 2014), and water inrush (Ricka et al. 2010), all of which can potentially damage mining equipment and/or cause physical injuries to mine workers A large number of inrush events occur worldwide during LW operations (Moebs and Sames 1989), especially in northern and eastern China, wherein landforms usually comprise thick unconsolidated layers. At the bottom of these unconsolidated layers lies an aquifer of unconsolidated sand, sandy gravel, and gravel under water pressures as high as 3–4 MPa. Several instances of water inrush have occurred (Table 1), seriously affecting mine safety and efficient production.

To avoid such hazards, the height of the water conducting fractured zone (WCFZ) must be accurately determined in advance. Conventional methods for calculating this height were established based on water body regulations concerning coal pillar design and extraction (Guo et al. 2018; Liu et al. 2014; Liu et al. 2018; Xu et al. 2016). An empirical formula applicable to different coal mines was established in the aforementioned regulations to determine the height of the WCFZ, but it ignored variations in rock mass strength. To make up for this deficiency, a method to predict the height of the WCFZ was developed by Xu (2016), in which the key stratum (KS) position must be accurately determined in advance. The basic premise of this method is that the KS position can be accurately determined.

The presently employed technique used to identify the KS position (Qian et al. 1996) focuses more on bedrock strata and ignores the effect of bearing structures within unconsolidated layers, which are usually represented as uniformly

✉ Jialin Xu
jlxucumt@163.com

1 State Key Laboratory of Mining Disaster Prevention and Control Co-founded by Shandong Province and the Ministry of Science and Technology, Shandong University of Science and Technology, Qingdao 266590, Shandong, China

2 College of Mining and Safety Engineering, Shandong University of Science and Technology, Qingdao 266590, Shandong, China

3 State Key Laboratory of Coal Resources and Safe Mining, China University of Mining and Technology, Xuzhou 221116, Jiangsu, China

4 School of Mines, China University of Mining and Technology, Xuzhou 221116, Jiangsu, China

Table 1 Water inrush hazards in eastern China when mining under unconsolidated confined aquifer

Longwall face	Length of LW face (m)	Mining height (m)	Time	Consequence of hazards
LW 1402(3), Panyi mine	155	3.7	1991-12-12	All chocks collapsed, water irruption quantity = 35 m^3/h
LW 17110(3), Pansan mine	130	3.3	1995-04-11	Roof of chocks 1 to 30 sank, the coal wall fell, all chocks collapsed, water irruption quantity = 18.5 m^3/h
LW 3222, Qidong mine	150	2.5	2001-11-25	All chocks collapsed, water irruption quantity 1520 m^3/h, mine flooding
LW 3221, Qidong mine	150	2.5	2002-12-15	33% of the chocks collapsed in the middle of a panel, water irruption quantity = 238.5 m^3/h
LW 7114, Qidong mine	174	2.6	2005-01-16	22 chocks collapsed, chocks severely damaged, water irruption quantity = 169 m^3/h
LW 7112, Qidong mine	85	2.6	2006-10-01	Chocks 21 to 56 collapsed, chocks severely damaged, water irruption quantity = 85 m^3/h
LW 7130, Qidong mine	88–134	3.7	2009-08-29	Roof of chocks 50 to 55 sank, water irruption quantity = 850 m^3/h
LW 6130, Qidong l mine	126	1.67	2010-01-24	Chocks 1 to 47 collapsed, water irruption quantity = 53 m^3/h
LW 7121, Qidong mine	129	1.96	2010-07-24	Chocks 1 to 40 collapsed,support hydraulic system badly damaged, shearer damaged, water irruption quantity = 50 m^3/h
LW 1602(3), Panyi mine	147.6	3.4	2010-09-26	Obvious strata problems, roof sank, all chocks collapsed, water irruption quantity = 6 m^3/h
LW 1202(3), Gubei mine	99.2	3.6	2011-05-16	All the safety valves of chocks opened, and most chocks collapsed
LW 3301, Xinhe mine	40	2.5	2012-01-07	Roof pressure intensified, some chocks collapsed, water irruption quantity = 1316 m^3/h
LW 7240, Renlou mine	75	2.5	2012-02-09	80% of the chocks collapsed, the motor of scraper conveyer near the tailgate was crushed, water irruption quantity = 20 m^3/h
LW 12041, Zhaogu mine	178.3	3.5	2012-04-02	Chocks 3 to 24 collapsed, roof sank, water irruption quantity = 280 m^3/h

distributed loading (UDL) structures with weights corresponding to those of unconsolidated layers. Any variations in loading stresses imposed on the strata due to the presence of an arch structure within unconsolidated layers (ASUL) are ignored. ASULs can form during excavation when unconsolidated layers are sufficiently thick, as is the case in a large number of coal mines in eastern and northern China. For example, the average thickness of unconsolidated layers in the Qidong coal mine is 363 m, with an average burial depth of the #7 coal seam measuring 460 m. Given these geological conditions, fracture characteristics of the overlying strata, determined without due consideration of the effects of ASUL, are unlikely to match those determined via field measurements (Xu et al. 2001). This is a particularly serious oversight, as a large number of coal mines in China (e.g. Xinjulong, Liangbaosi, Yuncheng, and Zhaolou mines) are prone to water inflow hazards (Zhu et al. 2016).

To address this concern, equivalent loads corresponding to unconsolidated layers can be calculated using a load reduction factor (LRF). These equivalent loads can be approximated as the product of LRF and the corresponding weights of the unconsolidated layers. Numerous empirical investigations, analytical derivations, and numerical modeling studies have been performed to evaluate the values of LRF in practical rock support designs for roadways, tunnels, and caverns (Einstein and Schwartz 1979; Heinz 1984; Kim et al. 2006; Muir Wood 1975; Panet and Guenot 1982). However, it is questionable whether LRF values used during rock stabilization could be adapted for use in unconsolidated layers, and only a few attempts have been made towards determining appropriate LRF values for unconsolidated layers in coal mining operations. There are two reasons behind such a paucity of such studies: (1) there are limited field data to facilitate the accurate monitoring of LRF; and (2) LRF values are influenced by the evolution of ASUL during coal mining. A theoretical equation for determining LRF values for unconsolidated layers was deduced by Huang (2005), based on the Terzaghi theory. That study found that LRF concerning unconsolidated layers were barely related to the lateral pressure ratio, thickness, and friction angle in unconsolidated layers, and any variations in strata loading caused by an ASUL could be ignored.

As use of this technique requires accurate determination of LRF caused by ASUL, a mechanical model of an ASUL was developed in this study to deduce the appropriate conditions for its formation. Fracture characteristics of KS, determined using the proposed ASUL model, were subsequently compared against those of unconsolidated layers simplified as UDL. A theoretical equation for LRF estimation has been derived based on the evolution of loading stresses imposed on KS. A modified process for KS identification involved in LRF determination is proposed, and theoretical results were verified using field observations obtained from LW 40106 of the Dafosi coal mine and LW 7130 of the Qidong coal mine, both in China.

Load Reduction Factor Determination

Bearing Structures in Overlying Strata

Arch Structure in Unconsolidated Layers (ASUL)

The ASUL model was established by comparing ASUL characteristics with those of a hingeless arch structure, assuming that: (1) the thickness of the cross section of the ASUL is constant; (2) the ASUL is subjected to uniformly distributed loading, which is equal to the weight of the unconsolidated layers above the ASUL; (3) the horizontal loading on the ASUL is also uniformly distributed, and the ratio of horizontal and vertical loading stress is defined as the lateral pressure ratio; and (4) the ASUL is not supported by the caved unconsolidated layers under the ASUL. ASULs form when the thickness of unconsolidated layers exceeds the sum of the rise and thickness of a potential ASUL. In accordance with Fig. 1, the critical thickness of unconsolidated layers is expressed as follows (Wang et al. 2019a, b)

$$\begin{cases} H_C = \frac{H_{arch}}{L_{arch}}\left(L_m - \frac{2\sum h}{\tan\alpha}\right) + \frac{\gamma h_0 H_{arch}}{\left[\gamma\left(h_0+H_{arch}\right)\tan(45°+\frac{\varphi}{2})+2C\right]\tan(45°+\frac{\varphi}{2})\cos\varphi} \\ \frac{H_{arch}}{L_{arch}} \geq \frac{\sqrt{\left(C+\gamma h_0\tan\varphi\right)^2+\lambda\gamma^2 h_0^2}-\gamma h_0\tan\varphi-C}{2\lambda\gamma h_0} \\ \delta_{arch} = \frac{\gamma h_0 L_{arch}}{\left[\gamma\left(h_0+H_{arch}\right)\tan(45°+\frac{\varphi}{2})+2C\right]\tan(45°+\frac{\varphi}{2})\cos\varphi} \end{cases} \quad (1)$$

wherein H_C is the critical thickness of unconsolidated layers for the ASUL; L_m denotes the mining width of the LW face; L_{arch}, H_{arch}, and δ_{arch} represent the span, rise, and thickness of the ASUL, respectively; h_0 denotes the thickness of the unconsolidated layers above the ASUL; λ is the lateral pressure ratio; Σh, α, and γ, represent the thickness, fracture angle, and unit weight of bedrock strata, respectively; and φ and C represent the friction angle and cohesion strength of unconsolidated layers, respectively.

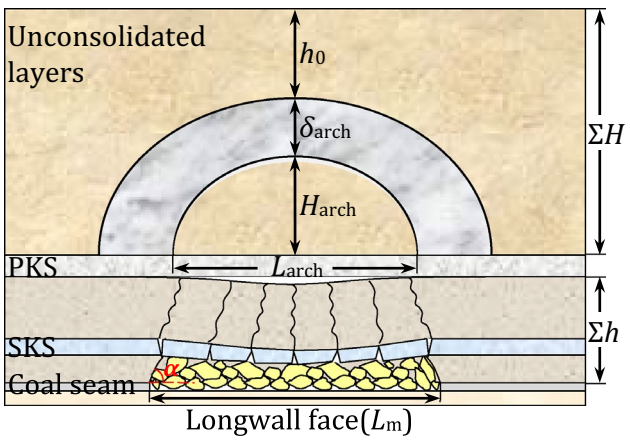

Fig. 1 Model of arch structure in unconsolidated layers

KS Structure in Bedrock

According to KS theory, the KS is a thick layer of rock capable of bearing the weight and controlling the movement of a part or the entire overlying strata. This implies that when a KS ruptures, part of or the entire strata above it would simultaneously subside. For greater specificity, the stratum that controls the movement of part of the overlying strata is named the sub-key stratum (SKS), while the stratum that controls the movement of the entire overlying strata is referred to as the primary key stratum (PKS). According to KS theory, the position of the KS can be identified based on stiffness and strength principles (Qian et al. 1996) given by:

$$\begin{cases} q_1|_{n+1} < q_1|_n \\ l_{n+1} > l_n \end{cases} \quad (2)$$

where $q_1|_{n+1}$ and $q_1|_n$ represent stresses applied to the (n + 1) th and nth layers, respectively, while l_{n+1} and l_n represent fracture intervals of the (n + 1)th and nth layers, respectively. A modified equation to calculate the loading on the uppermost hard stratum can be obtained as:

$$q_n = \frac{E_{n,0}h_{n,0}^3\left(\sum_{j=0}^{m_n} h_{n,j}\gamma_{n,j} + K\gamma H\right)}{\sum_{j=0}^{m_n} E_{n,j}h_{n,j}^3} \quad (3)$$

wherein ΣH and γ, respectively, represent the thickness and bulk density of unconsolidated layers. Subscript k in Eq. 3 represents the kth hard stratum from the seam level, while subscript j represents the jth soft stratum controlled by the kth hard stratum; m_k denotes the number of soft strata layers controlled by the kth hard stratum; and $E_{k,j}$, $h_{k,j}$, $\gamma_{k,j}$ respectively represent the elastic modulus, thickness, and bulk density of the jth soft stratum controlled by the kth hard stratum. With this modified process for KS identification, if the thickness of the unconsolidated layers is less than the critical thickness calculated using Eq. 1, LRF (K) equals unity, and the model can be treated as a traditional one (Qian et al. 1996). If, however, an ASUL is present within the unconsolidated layers, the value of LRF (K) needs to be derived in accordance with Eq. 3.

Simulation of KS Fracturing Under ASUL Effects

Simulation Models

Two comparative models were established to study the effects of an ASUL on PKS fractures. The first model, Model A, was based on an ASUL and measured 250 × 30 × 150 cm in length, width, and height (Fig. 2a). In Model B,

unconsolidated layers were replaced by UDL (Fig. 2b). Identical bedrock strata were used in both models. UDL was achieved by means of a regulating system comprising a pressurized cylinder, mobile pistons, and a servo pressure regulation system to maintain a stable loading of 13 kPa on the PKS during excavation. Fifteen stress gauges were placed on the PKS to monitor any change in loading conditions.

Scaled physical models were designed in accordance with laws of similarity theory (Eq. 4) (Ghabraie et al. 2015a, b; Yin et al. 2018).

$$\begin{cases} \frac{C_\sigma}{C_\rho \times C_L} = 1 \\ C_\sigma = \frac{\sigma_P}{\sigma_m}, C_\rho = \frac{\rho_P}{\rho_m}, C_L = \frac{L_P}{L_m} \end{cases} \quad (4)$$

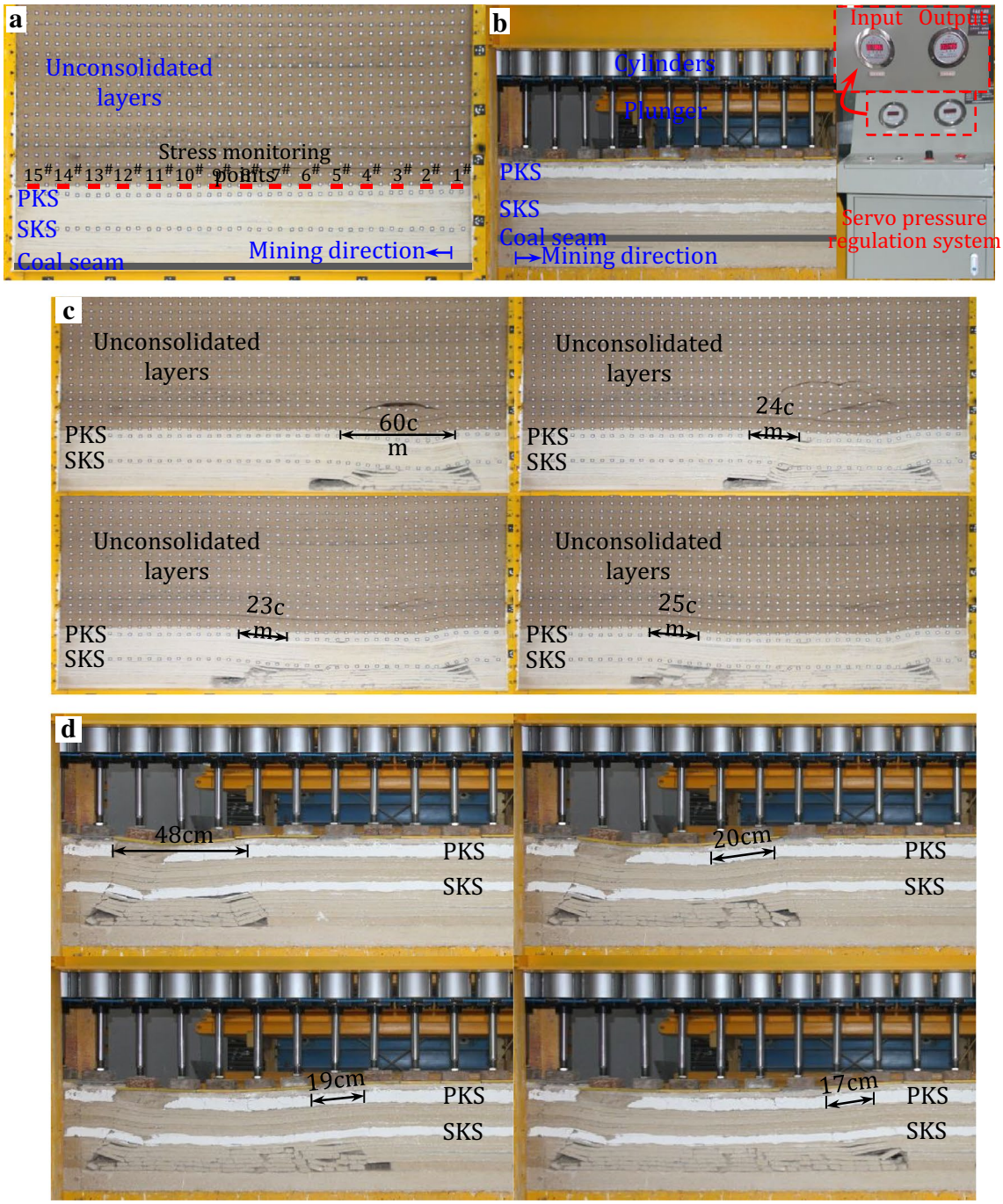

Fig. 2 Physical model and experimental results. **a** model with unconsolidated layers, **b** model without unconsolidated layers, **c** results of model (**a**), **d** results of model (**b**)

wherein C_σ, C_ρ, and C_L denote similarity constants for strength, density, and geometry, respectively. Subscripts P and m denote field conditions and the physical model of the prototype. Based on the dimensions of Model A, $C_L = 100:1$, $C_\rho = 1.67:1$, and $C_\sigma = 167:1$.

Materials used to simulate bedrock strata include sand, calcium carbonate, and gypsum (Ghabraie et al. 2015a). On the basis of trials performed to test unconsolidated layer parameters, a material comprising a 10:1 mass ratio mix of sand and dry sawdust was used in this study. Suitable mixtures for different overlying strata were determined by strength tests and are summarized in Table 2.

Characteristics of KS Fractures

Characteristics of KS fractures that were observed during the excavation operation performed as part of the physical simulation are listed below and illustrated in Fig. 2c, d.

1. In Model A comprising unconsolidated layers, the first PKS fracture interval measured 60 cm. Corresponding periodic intervals of PKS fractures in Model A measured 24, 23, and 25 cm, with an average value of 24 cm.
2. In Model B, the first PKS fracture interval measured 48 cm, and corresponding periodic intervals of KS fractures measured 20, 19, and 20 cm, with an average value of 19 cm.
3. When compared with results obtained using Model B, the PKS fracture interval in Model A was observed to increase during the first and subsequent fracture periods by 25% and 26%, respectively.

Evolution of KS Loading

KS fracture intervals are determined by the thickness, mechanical properties, and loading of the KS, with only the latter differing between Models A and B in this study. Thus, it is the loading imposed on the PKS that creates the different fracture intervals.

The evolution of loading on the PKS prior to the occurrence of its first fracture in Model A is illustrated in Fig. 3. Given the effects of ASUL, distribution of this loading can be divided into an original zone; a reduced stress zone above the gob area, wherein the stresses are observed to be less than the weight of the unconsolidated layers, and; an increased stress zone above both sides of the gob area, wherein the loading is greater than the weight of the unconsolidated layers. Stress loading above the gob area tends to gradually decrease with excavation, while the loading above both sides of the gob area tends to gradually increase. Therefore, the loading imposed on PKS in Model B tends to remain stable during excavation, since it bears the entire weight of the unconsolidated layers. This, however, is not realistic, since the PKS fracture interval tends to decrease during excavation.

An ASUL formed when the thickness of unconsolidated layers exceeds the critical thickness, calculated using Eq. 1, can cause PKS loading to exhibit dynamic variations and non-uniform distribution. Under such conditions, PKS loading cannot be approximated as UDL in the KS identification process, as would normally be the case in a conventional model. An LRF, therefore, must be determined in order to calculate the equivalent loading of unconsolidated layers; this, however, is influenced by evolution of the loading imposed on the PKS.

LRF Determination for Unconsolidated Layers

Loading curves depicted in Fig. 3 were simplified to the linear form for quantification by treating PKS as a traditional

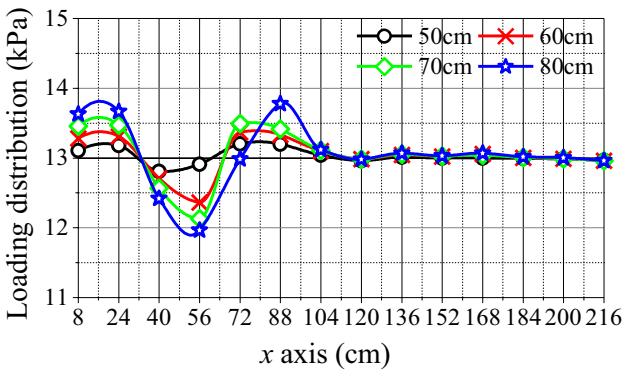

Fig. 3 Evolution of PKS loading

Table 2 Mechanical parameters of bedrock specimen

Rock strata	Material ratio sand: $CaCO_3$: gypsum	Bulk density kN/m^3	Elastic modulus MPa	Compressive strength KPa	Tensile strength KPa
Unconsolidated	–	12.2	0.93	30.3	3.3
PKS	50:3:7	16.4	131.7	222	30.5
KS	60:5:5	15.7	95.8	158	16.4
Soft rock	50:7:3	16.5	47.9	90	12.0
Coal seam	70:7:3	14.8	17.9	70	9.7

fixed-end beam (Fig. 4). The loading imposed on PKS comprised loading distribution functions, $Q_1(x)$ ($x \in (0, l_1)$), $Q_2(x)$ ($x \in (l_1, l_1+l_2)$), and $Q_3(x)$ ($x \in (l_1+l_2, l_1+l_2+l_3)$), expressed as:

$$\begin{cases} Q_1(x) = \frac{(q_{12}-q_0)}{l_1}x + q_0 \\ Q_2(x) = -\frac{q_{12}}{l_2}x + \frac{(l_1+l_2)q_{12}}{l_2} \\ Q_3(x) = \frac{q_3}{l_3}x - \frac{(l_1+l_2)q_3}{l_3} \end{cases} \quad (5)$$

where q_0 denotes the in situ stress; ($2\ l_3$) denotes ASUL span, determined in accordance with Fig. 5; (l_1+l_2) denotes ASUL thickness calculated using Eq. (1); q_3 denotes peak loading below the ASUL, which can be calculated by multiplying the rise in ASUL, in accordance with Eq. 1, caused by the bulk density of unconsolidated layers obtained via lab tests; and q_2 denotes peak loading at the ASUL abutment. This peak loading can be calculated using PKS load in accordance with the relation $\left(\int_0^{l_1} Q_1(x)dx + \int_{l_1}^{l_1+l_2} Q_2(x)dx + \int_{l_1+l_2}^{l_1+l_2+l_3} Q_3(x)dx = q_0(l_1+l_2+l_3)\right)$.

As depicted in Fig. 5, the PKS comprises fixed supports at both ends, thereby resulting in a statically indeterminate structure. The released structure at the symmetrical section C, depicted in Fig. 4, was selected as redundant, with a bending moment at the midpoint of X_1. This results in the

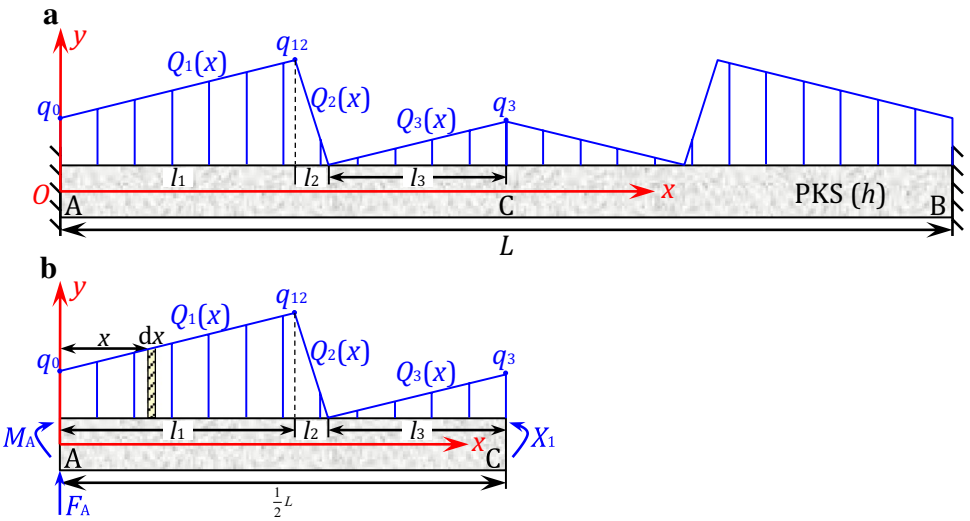

Fig. 4 Mechanical model to determine LRF. **a** Fixed-end beam mechanical model for primary key stratum fracture based on arch structure in unconsolidated layers, **b** Released structurewhen reaction at end *C* is the redundant

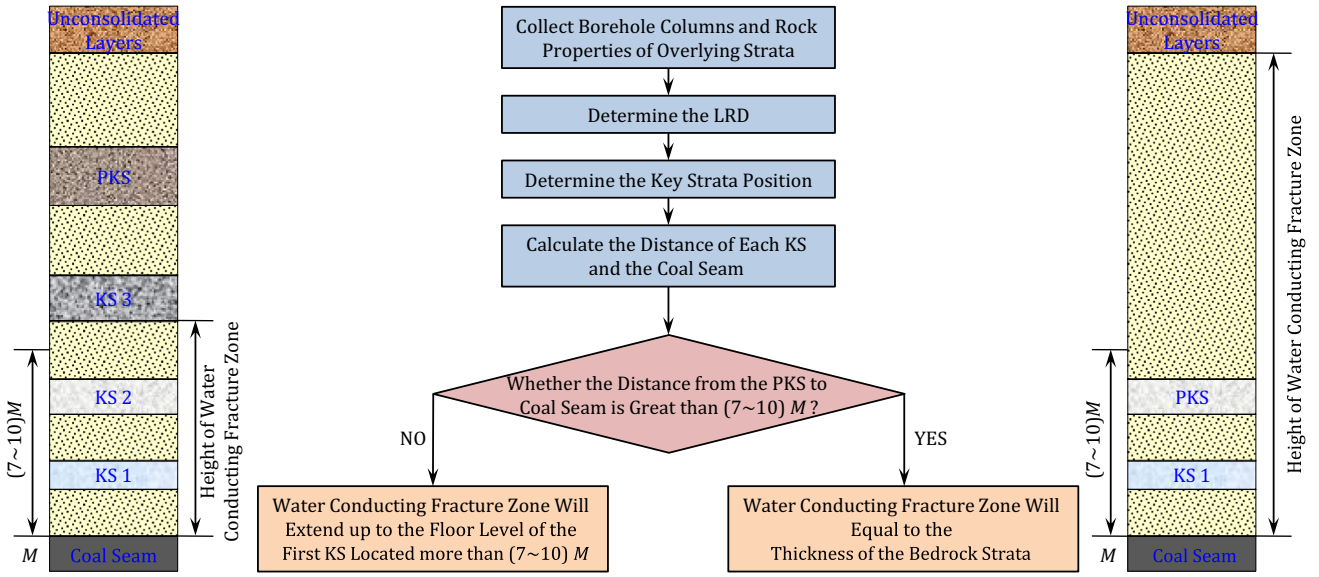

Fig. 5 Method to predict height of water conducting fractured zone

presence of two unknown reactions, M_A and F_A at the left end of the PKS structure, by which a regular force equation can be obtained:

$$\delta_{11}X_1 = \Delta_{1P} \tag{6}$$

wherein Δ_{1P} denotes PKS displacement under given loading, $\Delta_{1P} = \int \frac{\overline{M_1}\cdot M_P}{EI}dx$, $\delta_{11} = \int \frac{\overline{M_1}\cdot \overline{M_1}}{EI}dx$, $\overline{M_1}$ denotes the bending moment induced by X_1, $\overline{M_P}$ denotes the PKS bending moment under loading, E is the elastic modulus, and I represents the moment of inertia.

Using the equilibrium equation for bending moment about an axis passing through the cross section, we get

$$M_1(x) = \frac{(l_1-x)^2}{6}\left[\frac{(q_{12}-q_0)x}{l_1} + q_0 + 2q_{12}\right], x \in [0, l_1]$$

$$M_2(x) = \begin{cases} \frac{q_{12}l_2}{2}\left(\frac{l_2}{3} + l_1 - x\right), x \in [0, l_1] \\ \frac{(l_1+l_2-x)^3 q_{12}}{6l_2}, x \in [l_1, l_1+l_2] \end{cases}$$

$$M_3(x) = \begin{cases} \frac{q_3 l_3}{2}\left(\frac{2l_3}{3} + l_2 + l_1 - x\right), x \in [0, l_1+l_2] \\ -\frac{(l_1+l_2-2l_3-x)(l_1+l_2+l_3-x)^2 q_3}{6l3}, x \in [l_1+l_2, l_1+l_2+l_3] \end{cases} \tag{7}$$

Thus, the bending moment of PKS under the given loading comprising Q_1, Q_2, and Q_3 can be determined

$$M_P(x) = \begin{cases} \frac{(l_1-x)^2}{6}\left[\frac{(q_{12}-q_0)x}{l_1} + q_0 + 2q_{12}\right] + \frac{q_{12}l_2}{2}\left(\frac{l_2}{3} + l_1 - x\right) + \frac{q_3 l_3}{2}\left(\frac{2l_3}{3} + l_2 + l_1 - x\right), x \in [0, l_1] \\ \frac{(l_1+l_2-x)^3 q_{12}}{6l_2} + \frac{q_3 l_3}{2}\left(\frac{2l_3}{3} + l_2 + l_1 - x\right), x \in [l_1, l_1+l_2] \\ -\frac{(l_1+l_2-2l_3-x)(l_1+l_2+l_3-x)^2 q_3}{6l3}, x \in [l_1+l_2, l_1+l_2+l_3] \end{cases} \tag{8}$$

Substituting Eq. 8 into $\Delta_{1P} = \int \frac{\overline{M_1}\cdot M_P}{EI}dx$ yields:

$$\Delta_{1P} = \int_0^{l_1} \frac{\overline{M_1}\cdot M_{P1}(x)}{EI}dx + \int_{l_1}^{l_1+l_2} \frac{\overline{M_1}\cdot M_{P2}(x)}{EI}dx + \int_{l_1+l_2}^{l_1+l_2+l_3} \frac{\overline{M_1}\cdot M_{P3}(x)}{EI}dx \tag{9}$$

At the same time, the following equation can be derived:

$$\delta_{11} = \int_0^{l_1+l_2+l_3} \frac{\overline{M_1}\cdot \overline{M_1}}{EI}dx \tag{10}$$

By substituting Eqs. 9 and 10 in Eq. (6), the value of X_1 can be derived:

$$X_1 = \frac{1}{24(l_1+l_2+l_3)}\left\{\begin{array}{l}(q_0+3q_{12})l_1^3 + 6(q_{12}l_2+q_3l_3)l_1^2 + 4(l_2^2q_{12}+3q_3l_3l_2+2q_3l_3^2)l_1 \\ +l_2^3q_{12} + 6l_2^2l_3q_3 + 8l_2l_3^2q_3 + 3q_3l_3^3\end{array}\right\} \tag{11}$$

Using the equilibrium equation for the bending moment at the left end of the PKS, the following equation can be obtained:

$$M_A - X_1 + \frac{(q_{12}+q_0)}{2}\frac{1}{3}\frac{l_1(q_0+2q_{12})}{q_{12}+q_0} + \frac{1}{2}q_{12}l_2\left(l_1 + \frac{l_2}{3}\right) + \frac{1}{2}q_3l_3\left(l_1 + l_2 + \frac{2}{3}l_3\right) = 0 \tag{12}$$

On substituting Eq. 11 in Eq. 12, the bending moment M_A simplifies to:

$$M_A = (k_1q_0 + k_2q_{12} + k_3q_3)L^2 \tag{13}$$

wherein: $k_1 = \frac{(3l_1+4l_2+4l_3)l_1^2}{24L^2(l_1+l_2+l_3)}$, $k_2 = \frac{(l_1+l_2)(5l_1^2+9l_1l_2+8l_1l_3+4l_2l_3+3l_2^2)}{24L^2(l_1+l_2+l_3)}$, $k_3 = \frac{\left[5l_3^2+12(l_1+l_2)l_3+6(l_1+l_2)^2\right]l_3}{24L^2(l_1+l_2+l_3)}$.

Thus, the fracture interval of the PKS during its first fracture period can be deduced:

$$L = h\sqrt{\frac{2\sigma_T}{Kq_0}}, \left(K = \frac{12(k_1q_0+k_2q_{12}+k_3q_3)}{q_0}\right) \tag{14}$$

wherein σ_T represents the limited tension strength and K represents the LRF.

Unlike results previously obtained based on assumptions, PKS fracture intervals calculated using Eq. 14 were influenced by the LRF value. Under normal operating conditions in LW 7130 of the Qidong coal mine, the thickness of the unconsolidated layers measured 345.6 m, while that of the bedrock strata measured 52.62 m; the fracture angle of bedrock strata measured 60°; bulk density of the unconsolidated layers was 20 kN/m^3, the lateral pressure ratio was of the order of 3.0, and the friction angle and cohesion strength of the unconsolidated layers measured 7.5° and 1.0 MPa, respectively. These values yield an LRF of 0.66 in accordance with Eq. 14. As a result, the PKS fracture interval with ASUL was observed to be 1.2 times that of a traditional model (Qian et al. 1996). This was found to be consistent with the experimental data.

Method to Predict the Height of the Water Conducting Fractured Zone

The proposed KS identification method is based on the effect of KS on the height of the WCFZ (Xu 2016). According to this method, the height of the WCFZ can be determined in four steps (Fig. 5):

Step one: Collect borehole columns and rock properties of the overlying strata at different positions along the mining direction.
Step two: Determine the LRF considering the ASUL, according to Eq. 14. Determine the KS position in overburden strata using the KSPB software on the basis of borehole columns and rock properties collected in step one.
Step three: Calculate the distance between the KS and the roof interface of the coal seam. In this case, the critical height of the KS fracture can be estimated as 7–10 × M, where M represents the coal seam's thickness.
Step four: Determine the height of the WCFZ using the estimation criterion. When the distance between the PKS and the coal seam exceeds 7–10 × M, the WCFZ tends to extend up to the floor level of the first KS located more than 7–10 × M above the mining seam, thereby making the height of the WCFZ equal to the distance between the KS and the coal seam. When the PKS height above the coal seam is less than 7–10 × M, the height of the WCFZ equals or exceeds the thickness of the bedrock strata. This indicates the possibility of water inrush hazards during LW mining operations.

Field Verifications

Case 1: Longwall Face 40106 of the Dafosi Coal Mine

Longwall 40106 of the Dafosi coal mine, which is located in the Binchang mining area of Shanxi Province, measures 1916 m and 180 m in length and width, respectively (Fig. 6a). The coal seam is 11.5 m thick, on average. Furthermore, the thickness of the unconsolidated layers of LW 40106 averages 195 m, and the thickness of the bedrock strata averages 300 m. Thus, an ASUL can form during excavation, which in accordance with Eq. 3, yields an LRF of 0.75. By substituting this LRF into the implementation process of KS identification, the KS positions can be determined within the LW face (Fig. 6b).

Note that there are four KS layers within borehole D18, and the vertical distance between the coal seam and the PKS measures 197.6 m. With the distance between the PKS and the coal seam exceeding 7–10 × M, the WCFZ was observed to extend up to the floor level of the first KS located at a distance exceeding 7–10 × M above the mining seam, thereby making the height of the WCFZ equal to the distance between PKS and coal seam. The calculated height of the WCFZ, in this case, equals 197.6 m.

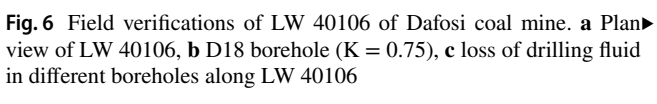

Fig. 6 Field verifications of LW 40106 of Dafosi coal mine. **a** Plan view of LW 40106, **b** D18 borehole (K = 0.75), **c** loss of drilling fluid in different boreholes along LW 40106

To verify these results, the actual height of the WCFZ was determined based on the loss of drilling fluid during borehole drilling (Fig. 6c). When the boundary of the WCFZ did not extend up to the bottom of the boreholes, the borehole walls remained smooth, and the surrounding rock masses within the borehole stayed intact without noticeable fracturing or borehole wall failure. As a result, the drilling fluid loss was minimal. When the bottom of the surface borehole advanced into the WCFZ, the loss of drilling fluid quickly increased.

Drilling fluid loss was observed to quickly increase in surface boreholes T1, T2, and T3 at depths of 298.5, 299.7, and 270.5 m, respectively, indicating boundary development of the WCFZ at those depths. Based on the depth of the coal seam in these three boreholes, the actual height of the WCFZ was observed to be 171.6, 170.8, and 192.1 m, respectively. Consequently, the height of the WCFZ was measured to be 192.1 m, which was consistent with the theoretical results calculated using the modified KS identification process (197.6 m).

Case 2: Longwall Face 7130 of the Qidong Coal Mine

Longwall 7130 of the Qidong coal mine, which is in the Wanbei mining area of Anhui Province, is 1638 m long (Fig. 7a). The width of LW 7130 varies from 88 to 172 m. Furthermore, the coal seam is 3.23 m thick, on average, and the average inclination of the coal seam is 12.5°. The thickness of the unconsolidated layers of LW 7130 ranges from 338.7 to 361.3 m, with the average thickness being 351 m, and the thickness of the bedrock strata averages 52 m. The LRF was determined to 0.66 using Eq. 14, and the KS positions were determined within the LW face (Fig. 7b, c).

Note that two KS layers exist in boreholes D5 and D6, and that the vertical distance between the coal seam and the PKS measured 31.88 and 30.46 m, respectively. The mining thickness was 2.85 and 2.83 m in boreholes D5 and D6, respectively. With the vertical distance between the PKS and the coal seam exceeding 7–10 × M, the WCFZ was determined to extend up to floor level of the first KS. This means that the height of the WCFZ should equal the distance between the KS and coal seam, which was determined to be 31.88 and 30.46 m in boreholes D5 and D6, respectively.

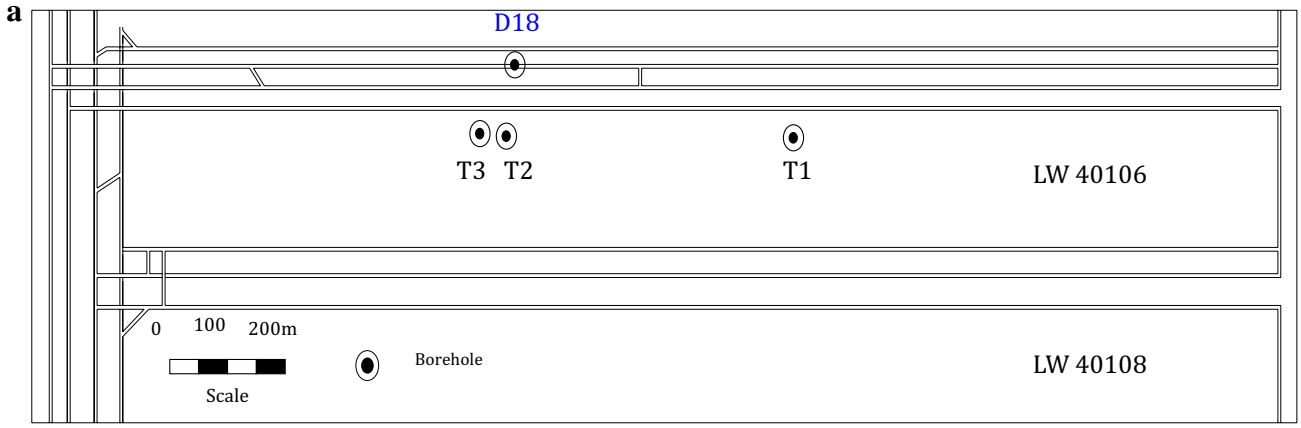

b

No.	Thickness (m)	Depth (m)	Lithology	Remarks
33	192.50	192.50	Unconsolidated layers	
32	98.51	291.01	Fine grained sandstone	PKS
31	21.26	312.27	Sandstone	
30	42.17	354.44	Silty mudstone	
29	5.24	359.68	Siltstone	
28	1.50	361.18	Sandstone	
27	6.89	368.07	Siltstone	
26	1.53	369.60	Sandstone	
25	1.47	371.07	Fine grained sandstone	
24	23.59	394.66	Sandstone	
23	2.00	396.66	Mudstone	
22	28.22	424.88	Fine grained sandstone	KS 3
21	3.76	428.64	Sandstone	
20	3.29	431.93	Mudstone	
19	0.73	432.66	Coal seam	
18	2.61	435.27	Mudstone	
17	8.03	443.30	Sandstone	KS 2
16	11.14	454.44	Silty mudstone	
15	1.56	456.00	Mudstone	
14	1.27	457.27	Coal seam	
13	0.85	458.12	Mudstone	
12	1.01	459.13	Coal seam	
11	1.46	460.59	Mudstone	
10	1.00	461.59	Coal seam	
9	1.90	463.49	Silty mudstone	
8	6.43	469.92	Silty mudstone	
7	0.88	470.80	Coal seam	
6	1.64	472.44	Mudstone	
5	5.30	477.74	Silty mudstone	
4	1.24	478.98	Siltstone	
3	6.67	485.65	Mudstone	
2	1.04	486.69	Fine grained sandstone	KS 1
1	1.90	488.59	Silty mudstone	
0	14.93	503.52	#4 coal seam	

c

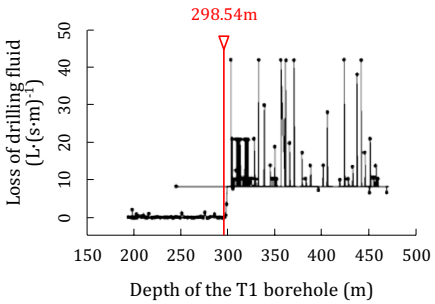

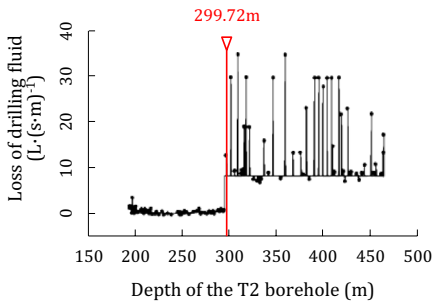

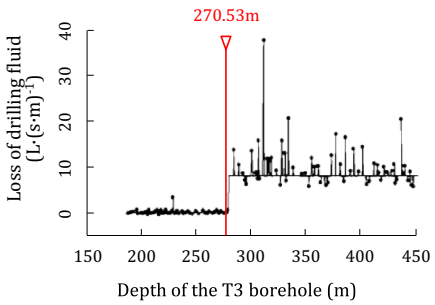

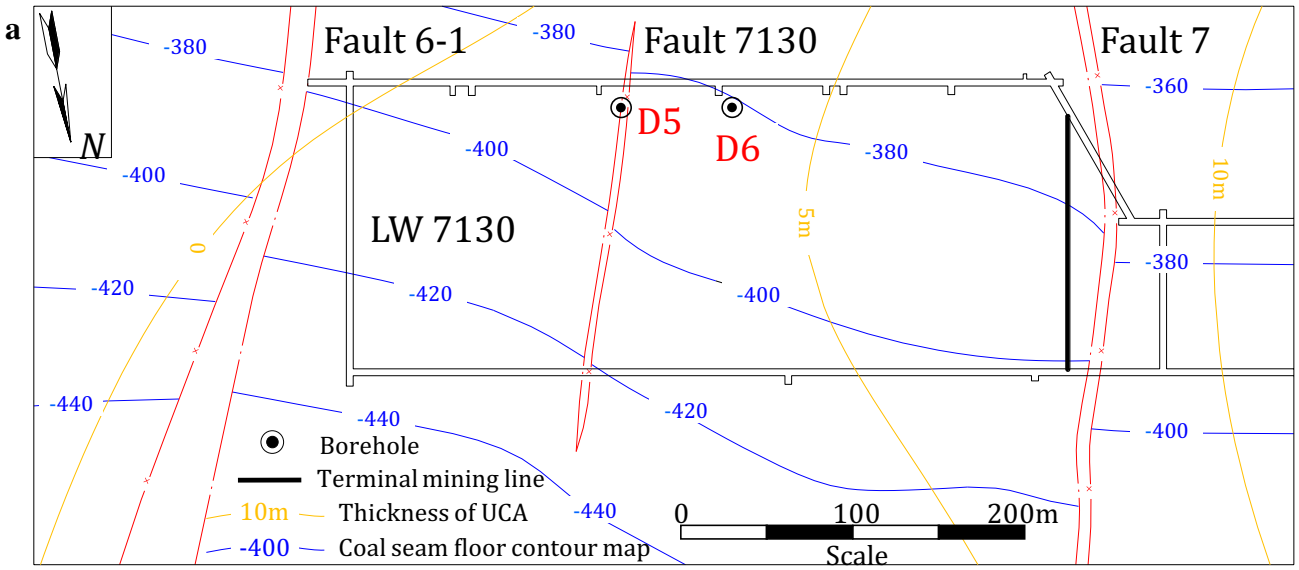

b

No.	Thickness (m)	Depth (m)	Lithology	Remarks	Column
16	342.6	342.60	Unconsolidated layers		
15	8.20	350.80	Mudstone		
14	3.80	354.60	Siltstone		
13	2.70	357.30	Mudstone		
12	2.20	359.50	Fine grained sandstone		
11	4.30	363.80	Mudstone		
10	3.25	367.05	Fine grained sandstone	PKS	
9	2.30	369.35	Mudstone		
8	0.50	369.85	#6$_1$ coal seam		
7	7.45	377.30	Mudstone		
6	3.10	380.40	#6$_2$ coal seam		
5	0.55	380.95	Mudstone		
4	1.60	382.55	Fine grained sandstone		
3	10.38	392.93	Mudstone		
2	3.50	396.43	Siltstone	KS	
1	2.50	398.93	Mudstone		
0	2.85	401.78	#7$_1$ coal seam		

31.88 m

c

No.	Thickness (m)	Depth (m)	Lithology	Remarks	Column
17	345.55	345.55	Unconsolidated layers		
16	6.00	351.55	Mudstone		
15	0.45	352.00	Coal seam		
14	5.05	375.05	Mudstone		
13	2.20	359.25	Siltstone		
12	2.25	361.50	Fine grained sandstone		
11	3.95	365.45	Mudstone		
10	1.95	367.40	#6$_1$ coal seam		
9	4.50	371.90	Mudstone		
8	6.50	378.40	Siltstone	PKS	
7	2.90	381.30	#6$_2$ coal seam		
6	6.45	387.75	Mudstone		
5	2.58	390.33	Siltstone		
4	5.58	395.91	Mudstone		
3	3.17	399.08	Fine grained sandstone	KS	
2	5.78	404.86	Mudstone		
1	4.00	408.86	Mudstone		
0	2.83	411.69	#7$_1$ coal seam		

30.46 m

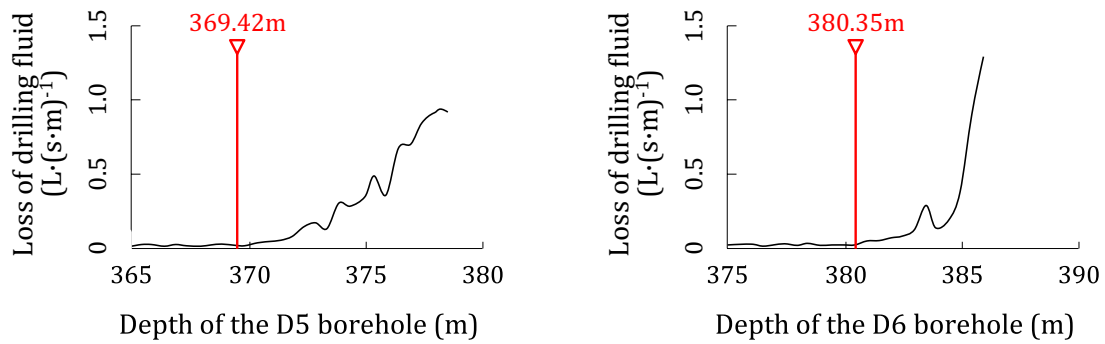

Fig. 7 Field verifications of LW 7130 of Qidong coal mine. **a** Plan view of LW 7130, **b** D5 borehole ($K = 0.66$), **c** D6 borehole ($K = 0.66$), **d** loss of drilling fluid in different boreholes along LW 7130

Based on the loss of drilling fluid at depths of 369.4 m and 380.9 m in those boreholes (Fig. 7d), the actual height of the WCFZ was observed to be 29.5 m and 28.5 m in boreholes D5 and D6, respectively. Therefore, the height of the WCFZ was determined to be 29.5 m, which was consistent with the results calculated using the modified KS identification processes (30.46 m).

Discussion

The conventional method for calculating the height of the WCFZ was established based on the regulations of coal pillar design and extraction for buildings, water bodies, railways, mine shafts, and roadways (State Bureau of Coal Industry 2000). An empirical formula for different overlying strata in coal mines was established to determine the height of the WCFZ in the aforementioned regulations (State Bureau of Coal Industry 2000). The height of the WCFZ in the empirical formula was determined based on the overlying strata lithology and mining height, but the mining height in the conventional formula is less than 3 m. Furthermore, the lithology of the roof strata is simply classified as hard rock, slightly hard rock, soft rock, and extremely soft rock, based on the statistical rules. Because of these conditions, the heights of the WCFZ as determined by the empirical formula do not match those determined through field measurements. More seriously, a number of coal mines in China are prone to significant mining-induced hazards, as shown in Table 1.

To make up for this deficiency, a method to predict the height of the WCFZ was developed by locating the KS. The application conditions of the new method are as follows: (1) The thickness of the unconsolidated layers is greater than the critical thickness given by the abovementioned equation, and the ASUL can form in the overlying strata; (2) There is at least one KS in the roof strata; (3) The new method is not suitable for multiple-seam mines. The reliability of the new method was verified by field observations performed in different coal mines, China. Comparison of results between different methods to predict height of WCFZ is depicted in Table 3 (Xu 2016).

In contrast to the results obtained using the conventional method, the height of the WCFZ based on the new method was closer to the field measurements. For example, since the vertical distance between the PKS and the coal seam exceeded $10 \times$M in boreholes D5, D6, and D8, the calculated heights of the WCFZ based on the new method was 31.9, 30.5, and 32.0 m, while the heights of the WCFZ were 29.5, 28.5, and 32.2 m, respectively. The error between the new method and field observations was -2.4 to ≈ 0.25 m, while the error between the conventional method and field observations was -15.2 to ≈ 9.2 m.

Using borehole D5 from LW face 7130 of the Qidong coal mine as an example, and the traditional method, the unconsolidated layers were represented as uniformly distributed loading structures with weights corresponding to those of the unconsolidated layers, and the KS position was determined as depicted in Fig. 8. There exists only one PKS layer within borehole D5, and the vertical distance between the coal seam and the PKS measured 2.5 m. Since the vertical distance between the PKS and the coal seam was less than $7–10 \times M$, the height of the WCFZ equals or exceeds the thickness of the bedrock strata. The height of the WCFZ measured 56.3 m in borehole D5. Using the modified method and considering the ASUL effects, the height of the WCFZ measured 31.88 m in borehole D5, which is consistent with those obtained by site observations (Fig. 7b). Therefore, the calculated height of the WCFZ was more accurate when ASUL was considered than when it was not.

Conclusions

1. The presence of an ASUL tends to restrict the downward movement of overlying strata and transfers loads to ASUL abutment during excavation. Consequently, the stress distribution can be divided into a reduced stress zone, an increased stress zone, and an original zone. A mechanical model to determine the LRF for unconsolidated layers was established by considering the load transfer effect due to ASUL according to physical simulations. The equivalent loading was derived by multiplying the LRF with the weight of the unconsolidated layers. The LRF values were influenced by the width of the LW face, thickness of the bedrock strata and unconsolidated layers, characteristics of the ASUL, and the strength of the unconsolidated layers.
2. A new method was proposed to predict the height of the WCFZ by determining the location of the KS involved in LRF, considering overburden load transfer under ASUL effects. A modified process for KS identification was proposed for the new method. When the distance between the PKS and coal seam is greater than $7–10 \times M$, where M refers to the coal mining height, the WCFZ tends to extend up to the floor level of the first KS, located approximately the same distance ($7–10 \times M$) above the mining seam, thereby making the height of the WCFZ equal to the distance between the KS and coal seam. When the vertical distance between the PKS and coal seam is less than $7–10 \times M$, the height of the WCFZ tends to be equal to or greater than the thickness of the bedrock strata.
3. The new method was verified by field observations made in coal mines in China. The application conditions of the

Table 3 Comparison of results between different methods to predict the height of water conducting fractured zone (Xu 2016)

Longwall face	Surface borehole	Coal seam thickness	Distance between PKS and coal seam	Thickness of bedrock strata	Conventional regulations		New method	Field observations	Error between conventional regulations and field observations		Error between new method and field observations
					State Bureau of Coal Industry 2000	State Bureau of Coal Industry 2000			State Bureau of Coal Industry 2000	State Bureau of Coal Industry 2000	
LW 40106 of Dafosi mine	D18	14.93	197.58	296.09	66.06–83.86	125.92	197.58	192.12	108.26–126.06	66.2	−5.46
LW 7114 of Qidong mine	D1	3.00	3.48	78.00	30.1–41.3	44.6	78.00	62.00	20.70–31.90	17.40	−16.00
	D2	3.00	3.48	116.00	30.1–41.3	44.6	116.00	102.30	61.00–72.20	57.70	−13.70
LW 7130 of Qidong mine	D5	2.85	31.88	58.33	29.3–40.5	43.7	31.88	29.51	−10.99 to 0.21	−14.19	−2.37
	D6	2.83	30.46	63.31	29.2–40.4	43.7	30.46	28.51	−11.89 to 0.69	−15.19	−1.95
LW 6130 of Qidong mine	D8	1.90	31.97	67.52	23.0–34.2	37.5	31.97	32.22	−1.98 to 9.22	−5.28	0.25
LW 7121 of Qidong mine	D9	2.30	7.49	89.16	26.0–37.2	40.3	89.16	66.48	29.28–40.48	26.18	−22.68
	D10	2.30	3.45	80.85	26.0–37.2	40.3	80.85	66.81	29.61–40.81	26.51	−14.04
LW 2302 of Xinglongzhuang mine	Dai15	2.50	38.58	79.45	27.3–38.5	41.6	38.58	42.00	3.40–14.70	0.40	3.42

No.	Thickness (m)	Depth (m)	Lithology	Remarks	Column
16	342.6	342.60	Unconsolidated layers		
15	8.20	350.80	Mudstone		
14	3.80	354.60	Siltstone		
13	2.70	357.30	Mudstone		
12	2.20	359.50	Fine grained sandstone		
11	4.30	363.80	Mudstone		
10	3.25	367.05	Fine grained sandstone		
9	2.30	369.35	Mudstone		
8	0.50	369.85	#6$_1$ coal seam		
7	7.45	377.30	Mudstone		
6	3.10	380.40	#6$_2$ coal seam		
5	0.55	380.95	Mudstone		
4	1.60	382.55	Fine grained sandstone		
3	10.38	392.93	Mudstone		
2	3.50	396.43	Siltstone	PKS	
1	2.50	398.93	Mudstone		
0	2.85	401.78	#7$_1$ coal seam		

Fig. 8 KS position determined of D5 borehole using the traditional method

new method are: the thickness of the unconsolidated layers must be greater than the critical thickness given by the abovementioned equation; an ASUL can form in the overlying strata; and there is at least one KS in the roof strata. The new method is not suitable for multiple-seam mines.

Acknowledgments This research was supported by the project supported by the National Natural Science Foundation of China (51904162), Shandong Provincial Natural Science Foundation, China (ZR2018BEE001), the Taishan Scholars Project, and the Scientific Research Foundation of SDUST for Recruited Talents (2017RCJJ006). We thank Editage [http://www.editage.cn] for English language editing. Thanks also to the anonymous reviewers for their constructive comments and suggestions.

References

Cai W, Dou LM, Gong SY, Li ZL, Yuan SS (2015) Quantitative analysis of seismic velocity tomography in rock burst hazard assessment. Nat Hazards 75(3):2453–2465

Einstein HH, Schwartz CW (1979) Simplified analysis for tunnel supports. J Geotech Eng Div 105:499–518

Fisne A, Esen O (2014) Coal and gas outburst hazard in Zonguldak Coal Basin of Turkey, and association with geological parameters. Nat Hazards 74(3):1363–1390

Ghabraie B, Ren G, Zhang X, Smith J (2015a) Physical modelling of subsidence from sequential extraction of partially overlapping longwall panels and study of substrata movement characteristics. Int J Coal Geol 140:71–83

Ghabraie B, Ren G, Smith J, Holden L (2015b) Application of 3D laser scanner, optical transducers and digital image processing techniques in physical modelling of mining–related strata movement. Int J Rock Mech Min Sci 80:219–230

Guo HJ, Ji M, Chen K, Zhang ZL, Zhang YD, Zhang ML (2018) The feasibility of mining under a water body based on a fuzzy neural network. Mine Water Environ 37(4):703–712

Heinz HK (1984) Applications of the new Austrian tunnelling method in urban areas. M.Sc. Thesis, Department of civil engineering, University of Alberta

Huang QX (2005) Studies on load-transmitting factor of thick sandy soil layer on key roof stratum in shallow seam mining. Chin J Geotech Eng 27(6):672–676

Kim HJ, Eisenstein Z, Chae BG, Jeong CH (2006) Estimates of stress reduction factors for the tunnel design. Tunn Undergr Space Technol 21(3):451–456

Liu YF, Wang SD, Wang XL (2014) Development characteristics of water flowing fractured zone of overburden deep buried extra thick coal seam and fully-mechanized caving mining. J China Coal Soc 39(10):1970–1976

Liu SL, Li WP, Wang QQ (2018) Height of the water-flowing fractured zone of the Jurassic coal seam in northwestern China. Mine Water Environ 37(2):312–321

Moebs NM, Sames GP (1989) Water—a hazard and a nuisance. Coal 26(10):60–63

Muir Wood AM (1975) The circular tunnel in elastic ground. Geotechnique 25(1):115–127

Panet M, Guenot A (1982) Analysis of convergence behind the face of a tunnel. Tunnelling, the Institution of Mining and Metallurgy, pp 197–204

Qian MG, Miao XX, Xu JL (1996) Theoretical study of key stratum in ground control. J China Coal Soc 21(3):225–230

Ricka A, Kuchovsky T, Sracek O, Zeman J (2010) Determination of potential mine water discharge zones in crystalline rocks at Rozna, Czech Republic. Environ Earth Sci 60(6):1201–1213

State Bureau of Coal Industry (2000) Regulations of coal pillar design and extraction for buildings, water bodies, railways, main shafts and roadways. Coal Industry Press, Beijing

Wang F, Jiang BY, Chen SJ, Ren MZ (2019a) Surface collapse control under thick unconsolidated layers by backfilling strip mining in coal mines. Int J Rock Mech Min Sci 113:268–277

Wang F, Xu JL, Xie JL (2019b) Effects of arch structure in unconsolidated layers on fracture and failure of overlying strata. Int J Rock Mech Min Sci 114:141–152

Xu JL (2016) Distribution law of mining-induced strata fractures and its applications. China University of Mining and Technology Press, Xuzhou

Xu JL, Qian MG, Ma WD, Zhao HY (2001) Discussion on load problem in physical and numerical simulation of strata movement. J China Univ Min Tech 30(3):252–255

Xu DJ, Peng SP, Xiang SY, Liang MX, Liu WM (2016) The effects of caving of a coal mine's immediate roof on floor strata failure and water inrush. Mine Water Environ 35(3):337–349

Xuan DY, Xu JL (2014) Grout injection into bed separation to control surface subsidence during longwall mining under villages: case study of Liudian coal mine, China. Nat Hazards 73(2):883–906

Yin DW, Chen SJ, Liu XQ, Ma HF (2018) Effect of joint angle in coal on failure mechanical behavior of roof rock-coal combined body. Q J Eng Geol Hydroge 51(2):202–209

Zhu ST, Feng Y, Jiang FX (2016) Determination of abutment pressure in coal mines with extremely thick alluvium stratum: a typical kind of rockburst mines in China. Rock Mech Rock Eng 49(5):1943–1952